# Solution Structure of BmKK4, the First Member of Subfamily α-KTx 17 of Scorpion Toxins[†,‡]

Naixia Zhang,[§,⊥] Xiang Chen,[§,⊥] Minghua Li,[∥] Chunyang Cao,[§] Yuefeng Wang,[§] Gong Wu,[§] Guoyuan Hu,[∥] and Houming Wu*[,§]

*State Key Laboratory of Bio-organic and Natural Products Chemistry, Shanghai Institute of Organic Chemistry, Chinese Academy of Sciences, Shanghai 200032, and State Key Laboratory of Drug Research, Shanghai Institute of Materia Medica, Shanghai Institutes for Biological Sciences, Chinese Academy of Sciences, Shanghai 200031, People's Republic of China*

*Received May 8, 2004; Revised Manuscript Received July 29, 2004*

ABSTRACT: BmKK4 is a 30 amino acid peptide purified from the venom of the Chinese scorpion *Buthus martensi* Karsch. It has been classified as the first member of scorpion toxin subfamily α-KTx 17. The 3D structure of BmKK4 in solution has been determined by 2D NMR spectroscopy. This toxin adopts a common α/*β*-motif, but shows a distinctive local conformation. The most novel feature is that the regular arrangements of the side chains of the residues involved in the *β*-sheet of BmKK4 are distorted by a classic *β*-bulge structure, which involves two residues (Asp18 and Arg19) in the first strand opposite a single residue (Tyr26) in the second strand. The bulge produces two main changes in the structure of the antiparallel *β*-sheet: (1) It disrupts the normal alteration of the side chain direction; the side chain of Asp18 turns over to form a salt bridge with that of Arg19. (2) It accentuates the twist of the sheet, and alters the direction of the antiparallel *β*-sheet. The unusual structural feature of the toxin is attributed to the shorter peptide segment (Leu15−Arg19) between the third and fourth Cys residues and two unique residues (Asp18 and Arg19) at the position preceding the fourth Cys. In addition, the lower affinity of the peptide for the Kv channel is correlated to the structural features: residue Arg19 instead of a Lys residue at the critical position for binding and the salt bridge formed between residues Arg19 and Asp18.

Potassium ($K^+$) channels play crucial roles in regulating a variety of cellular processes. Molecular cloning studies in recent decades have revealed enormous molecularly and functionally diverse $K^+$ channels with different physiological and pharmacological properties (*1*). Investigation of the structure and function of $K^+$ channels highly depends on the discovery of specific inhibitors, particularly neurotoxins isolated from marine and terrestrial organisms. Scorpion venoms are rich sources of fascinating toxic peptides, which bind with high affinity and specificity to various $K^+$ channels and thus have been successfully used to characterize $K^+$ channels (*2*−*8*). To date, a large number of $K^+$ channel toxins have been isolated as native peptides from various scorpion venoms, while a variety of toxins were identified by their cDNA sequences (*9*, *10*). Mainly according to their primary structures, these so-called short-chain scorpion peptides (23−43 amino acid residues) specific for $K^+$ channels have been divided into α-, *β*-, and *γ*-KTx families (*11*, *12*). The α-KTx's, which have been proven to be useful tools for probing the structural and functional characteristics of $K^+$ channels, are further classified into 19 subfamilies (*11*, *13*−*15*). Meanwhile, pharmacological studies showed that the $K^+$ channel specific scorpion toxins interact with four major classes of $K^+$ channels: voltage-gated (Kv-type),[1] high-conductance $Ca^{2+}$-activated (BK-type), small-conductance $Ca^{2+}$-activated (SK-type), and human *ether-a-go-go*-related gene (HERG-type). By mutation analysis of both $K^+$ channels and scorpion toxins, the interacting surface of scorpion toxins with $K^+$ channels has been described, and the receptor counterparts for some of the critical residues of the toxins were also identified (*16*−*19*). In addition, the successful building of the models of scorpion toxin/$K^+$ channel complexes have also given further insight into the interaction mode of scorpion toxins with $K^+$ channels (*20*−*21*). Despite the amount of work that has been done and the fact that some achievements have been obtained on the subject, the interacting surface areas between the $K^+$ channels and scorpion toxins are still an open question due to the diversity of both of them. Meanwhile, although short-chain scorpion peptides adopt a common global folding of the α/*β*-scaffold (*22*−*31*), the faces of the α/*β*-scaffold that interact with $K^+$ channels are not unique. Characterizing the structure and function of new $K^+$ channel specific scorpion toxins, which belong to a different subfamily and show distinct structural and functional characteristics, will provide very

[†] This work was supported by the National Science Foundation of China (Grant No. 20132030) and Chinese Academy of Sciences (Grant No. KGCX2-SW-213-05).

[‡] The atomic coordinates of BmKK4 have been deposited in the Brookhaven Protein Data Bank as entry 1S8K.

* To whom correspondence should be addressed. Fax: 86-21-64166128. Phone: 86-21-64163300, ext 1431. E-mail: hmwu@mail.sioc.ac.cn.

[§] Shanghai Institute of Organic Chemistry.

[∥] Shanghai Institutes of Biological Sciences.

[⊥] These authors contributed equally to this work.

[1] Abbreviations: 1D, one-dimensional; 2D, two-dimensional; 3D, three-dimensional; DQF-COSY, double-quantum-filtered shift-correlated spectroscopy; Kv channel, voltage-gated potassium channel; NMR, nuclear magnetic resonance; NOESY, nuclear Overhauser enhancement spectroscopy; RMSD, root-mean-square deviation; TOCSY, total correlation spectroscopy.

10.1021/bi0490643 CCC: $27.50 
Published on Web 09/04/2004

useful information for fully understanding the interaction between scorpion toxins and $K^+$ channels (*6*).

BmKK4 is isolated from the venom of the Chinese scorpion *Buthus martensi* Karsch (*32*). The primary sequence of BmKK4 is unique with a shorter peptide segment (only five residues) between the third and fourth Cys residues and the presence of two unusual residues (Asp and Arg) preceding the fourth Cys residue as compared with that of other short-chain scorpion toxins. It has been classified as the first member of the scorpion $K^+$ channel toxin subfamily α-KTx 17 (*13*). The action of BmKK4 on voltage-dependent potassium currents has been examined in acutely dissociated hippocampal neurons of rat (*33*). Here we report the three-dimensional solution structure of BmKK4 determined by NMR spectroscopy, which reveals some novel features of this molecule. The correlation of the 3D structure and its affinity for the Kv channel is also discussed.

## MATERIALS AND METHODS

All chemicals and reagents, unless otherwise stated, were purchased from Sigma.

*NMR Experiments*. The sample of BmKK4 used in this study was isolated from the venom of the Chinese scorpion *B. martensi* Karsch as described previously (*32*). The peptide BmKK4 was dissolved in $H_2O/D_2O$ (90/10 v/v) or 100% $D_2O$, pH 3.02 or 3.66, uncorrected for isotope effects, adjusted by adding 1 μL of dilute DCl or NaOD. The final concentration of BmKK4 was about 3.0 mmol/L. The amide proton exchange rate was determined after lyophilization and dissolution in 100% $D_2O$.

All the NMR experiments were recorded at 303 K on a Varian unity Inova 600 spectrometer. The experiments were performed at two pH values (3.02 and 3.66) to solve assignment ambiguities. Quadrature detection was employed in all experiments and the carrier frequency always maintained at the solvent resonance. Presaturation was used to suppress the water peak in all experiments. 2D DQF-COSY, TOCSY, and NOESY spectra were achieved in phase-sensitive mode by using the time-proportional phase incrementation method. All 2D NMR spectra were recorded with 4K data points in the $t_2$ dimension and 512 data points in the $t_1$ dimension. The TOCSY spectra were recorded using the MLEV-17 pulse sequence with mixing times of 80 and 120 ms. The NOESY spectra were acquired using mixing times of 200 and 300 ms, respectively. To determine slowly exchanging amide protons, a series of 1D spectra were recorded at 303 K during the first 2 h after the sample was dissolved in $D_2O$. A shifted sine window function and zero filling were applied prior to Fourier transformation. All experimental data were acquired and processed using the Vnmr 6.1B program on a SUN Sparc station 4 computer. The processed data were analyzed with XEASY for NMR spectrum visualization, peak picking, and peak integration on a Silicon Graphics Indigo R 5000 computer.

*Assignment Strategy and Structure Calculation.* The identification of amino acid spin systems and the sequential assignment were done using the standard strategy described by Wüthrich (*34*).

The NOESY (200 ms) spectrum was used to generate the distance constraints. Dihedral angle constraints were derived from $^3J_{HNH\alpha}$ coupling constants, which were obtained by analyses of the 1D $^1H$ NMR spectrum. Additional constraints were used to enforce hydrogen bonds implicated by the H−D exchange spectra. Distance geometry calculations were performed with the target function program DYANA on a Silicon Graphics Indigo II computer. The 35 structures with the lowest constraint violations were subjected to restrained energy minimization (REM) performed with the AMBER 5.0 package. The 25 best conformers with the lowest energy were used to represent the solution conformation of BmKK4. The programs PROCHECK and PROCHECK_NMR were used to evaluate the NMR structures of BmKK4. In addition, 3D conformations were produced with the MOLMOL program for visual comparison of the structures on a Silicon Graphics Indigo II computer. For pairs of conformers, RMSD values for various subsets of atoms were calculated. The mean solution structure was obtained by superimposing the 25 lowest energy AMBER conformers and then averaging the Cartesian coordinates of the corresponding atoms in the 25 superimposed conformers.

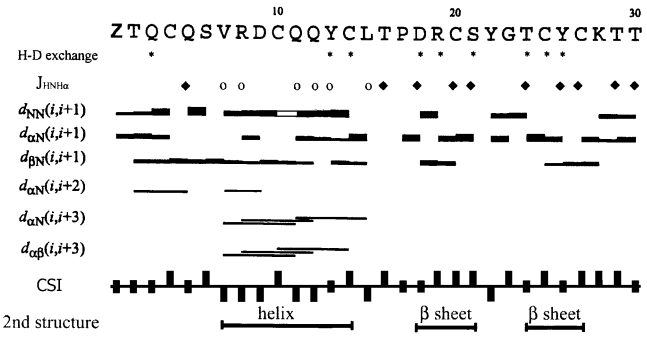


FIGURE 1: Summary of NOE connectivities, *J* coupling constant $^3J_{HNH\alpha}$, and the slowly exchanging amide protons. The thickness of the bar indicates the intensity of the NOEs. Asterisks represent the NH protons in slow exchange. *J* coupling constants $^3J_{HNH\alpha}$ are smaller than 6.0 Hz (open circles) and bigger than 8 Hz (filled tilted squares).

## RESULTS

*NMR Resonance Assignment*. The spin systems were identified on the basis of the DQF-COSY and TOCSY spectra. The fingerprint region of the DQF-COSY spectra recorded in $H_2O$ showed most of the HN−Hα cross-peaks, and the TOCSY spectra then were used to correlate the HN−Hα cross-peaks with their side chain spin systems for each residue.

The spin systems were connected in sequence by virtue of $d_{\alpha N}$, $d_{NN}$, and $d_{\beta N}$ connectivities in well-dispersed NOESY spectra. The unique residues Val7, Leu15, Gly23, and Lys28 in the sequence of BmKK4 were used as the entry points for the sequential assignment. Starting from these four amino acids, the sequential assignments of the segments Pyr1−Leu15 and Tyr22−Thr30 were obtained via $d_{\alpha N}(i,i+1)$, $d_{NN}(i,i+1)$, and $d_{\beta N}(i,i+1)$ connectivities. Then residue Ser21 was used as the starting point for the sequential assignment of the segment Pro17−Ser21 by the $d_{\alpha N}(i,i+1)$, $d_{NN}(i,i+1)$, and $d_{\beta N}(i,i+1)$ correlation peaks. The remaining Thr residue was assigned as Thr16. The sequential connectivities are illustrated in Figure 1. In addition, the medium-range NOE contacts such as $d_{\alpha N}(i,i+3)$ and $d_{\alpha\beta}(i,i+3)$ and coupling constants $^3J_{HNH\alpha}$, as well as the slowly exchanging NH protons, are also summarized in Figure 1.

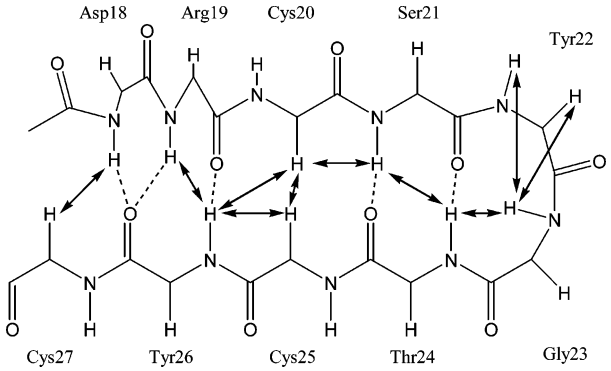


FIGURE 2: Antiparallel $\beta$-sheet secondary structure in BmKK4. Arrows indicate sequential and long-range NOEs. Dotted lines stand for hydrogen bonds identified on the basis of slowly exchanging amide protons and the interstrand NOEs.

*Hydrogen Bonds*. A total of nine (Gln3, Tyr13, Cys14, Asp18, Arg19, Ser21, Thr24, Cys25, and Tyr26) amide protons, which are still visible after H/D exchanging for 2 h, are considered as being engaged in hydrogen bonds (Figure 1). The acceptors of hydrogen bonds for the slowly exchanged amide protons were identified during the structure refinement.

*Coupling Constants*. Sixteen $^3J_{HNH\alpha}$ coupling constants were measured by the well-resolved $^1$H NMR spectrum and were converted into dihedral angle restraints (Figure 1).

*Secondary Structure*. Secondary structural elements of BmKK4 were identified using the unique NOE contacts and $^3J_{HNH\alpha}$ coupling constants. A continuous set of strong $d_{NN}(i,i+1)$ NOEs was observed in the segment of Val7 to Cys14, indicating a helical element. The deduction was supported by a series of medium-range $d_{\alpha N}(i,i+3)$ and $d_{\alpha\beta}(i,i+3)$ NOEs in this region. Further corroborative data came from $^3J_{HNH\alpha}$ coupling constants and slowly exchanging amide protons. Most of the $^3J_{HNH\alpha}$ coupling constants in the region of residues 7−14 are smaller than 6.0 Hz. The amide protons of residues Tyr13 and Cys14 are in slow exchange (Figure 1). Besides, the chemical shifts of α-protons for most of the residues in this region move upfield. These data further confirmed the above assignment of the helical structure.

In addition, strands Asp18−Ser21 and Thr24−Cys27 showed strong sequential $d_{\alpha N}$ connectivities, and the residues in these strands showed large $^3J_{HNH\alpha}$ (>8.0 Hz) coupling constants. Meanwhile, a network of long-range $d_{\alpha N}$, $d_{\alpha\alpha}$, and $d_{NN}$ NOEs were observed between these two strands, such as $d_{\alpha\alpha}$(Cys20,Cys25), $d_{\alpha N}$(Cys20,Tyr26), $d_{\alpha N}$(Cys27,Asp18), and $d_{NN}$(Arg19,Tyr26), as shown in Figure 2. These observations suggested the presence of an antiparallel double-stranded $\beta$-sheet. The location of the $\beta$-sheet secondary structure was also confirmed by the chemical shift index of the α-protons and the slowly exchanging amide proton data. As shown in Figure 1, the amide protons of residues Asp18, Arg19, Ser21, Thr24, and Tyr26 involved in the $\beta$-sheet are slowly exchanged. The hydrogen-bound partner of the amide proton of Asp18, Arg19, Ser21, Thr24, and Tyr26 was identified as being the carbonyl oxygen of Tyr26, Thr24, Ser21, and Arg19, respectively, during the structure refinement. The strands Asp18−Ser21 and Thr24−Cys27 were connected by a type I′ $\beta$-turn comprised of residues Ser21−Thr24. The latter was confirmed by $d_{NN}$(Tyr22,Gly23), as well as $d_{NN}$(Gly23,Thr24). In addition, the disulfide bridges were established from the dipolar interactions between the $\beta$-protons of relevant Cys residues.

*Structure Determination*. The input for the distance geometry calculations with the program DYANA consisted of upper distance limits derived from NOESY (mixing time 200 ms) cross-peak intensities using the program CALIBA, and dihedral angle constraints obtained from an initial interpretation of the vicinal coupling constants $^3J_{HNH\alpha}$. For the calibration of proton−proton distance limits ($r$ versus the cross-peak intensities), the dependence of $1/r^6$ was used for all protons. The calibration curves were refined on the basis of plotting cross-peak volume versus average proton−proton distance according to the preliminary structures. A total of 282 distance constraints were used (129 intraresidue, 64 sequential, 44 medium-range, and 45 long-range NOEs). Sixteen Φ angle constraints ($-55 \pm 15°$ for $^3J_{HNH\alpha} < 6.0$ Hz, $-120 \pm 35°$ for $^3J_{HNH\alpha} > 9.0$ Hz, and $-120 \pm 45°$ for 9.0 Hz > $^3J_{HNH\alpha}$ > 8.0 Hz) were used for structure calculation. In addition, nine distance constraints were added for three disulfide bonds (three per bond). Nine slowly exchanging amide protons were determined from the H−D exchanging experiments. Four of them were used to generate hydrogen bond constraints, which were imposed between slowly exchanging amide protons and their receptors on the basis of the DYANA preliminary structures. For each hydrogen bond, two limit restraints were used between the NH−O (0.22 nm) and N−O (0.32 nm) atom pairs. In addition, the program GLOMSA was used to obtain five stereospecific assignments of methylene protons on the basis of the preliminary structures. Totally, 315 constraints (average 10.5 constraints per residue) were obtained and used in the structure calculations of BmKK4.

Starting from 200 random structures, the 35 preliminary structures with the lowest target functions resulting from distance geometry calculations were subjected to simulated annealing and restrained energy minimization (REM) using the SANDER module of the AMBER 5.0 package. A cutoff radius of 0.8 nm for nonbonded interactions, with a residue-based pair-list routine, was used in all calculations. The force constants for distance restraints in EM were 500 kJ mol$^{-1}$ nm$^{-2}$. Energy minimization was performed using a combination of steepest descent and conjugate gradient algorithms with a gradient convergence norm of less than $10^{-4}$ kJ mol$^{-1}$ nm$^{-1}$. After energy minimization with AMBER, the 25 best DYANA conformers with the lowest energy are used to represent the solution conformation of BmKK4.

*Structure Description*. Figure 3a represents the superposition of the polypeptide backbones of the 25 best conformers. No NOE violations larger than 0.20 Å and no angle violations larger than 5° can be found. The overall agreement among individual conformers is indicated by global root-mean-square deviation (RMSD). The final set of 25 structures display an overall RMSD of 1.09 Å for the backbone atoms and 1.87 Å for all heavy atoms. The RMSD values for the backbone atoms and heavy atoms are decreased to 0.35 and 1.38 Å, if the first residue and last two residues of the toxin are not taken into consideration. Analysis of the ensemble of 25 structures using PROCHECK_NMR reveals that 77.8% and 19.7% of the residues lie in the most favored and allowed regions of the Ramachandran $\phi$, $\psi$ dihedral angle plot, respectively. The structural statistics for 25 conformers of the toxin are summarized in Table 1.

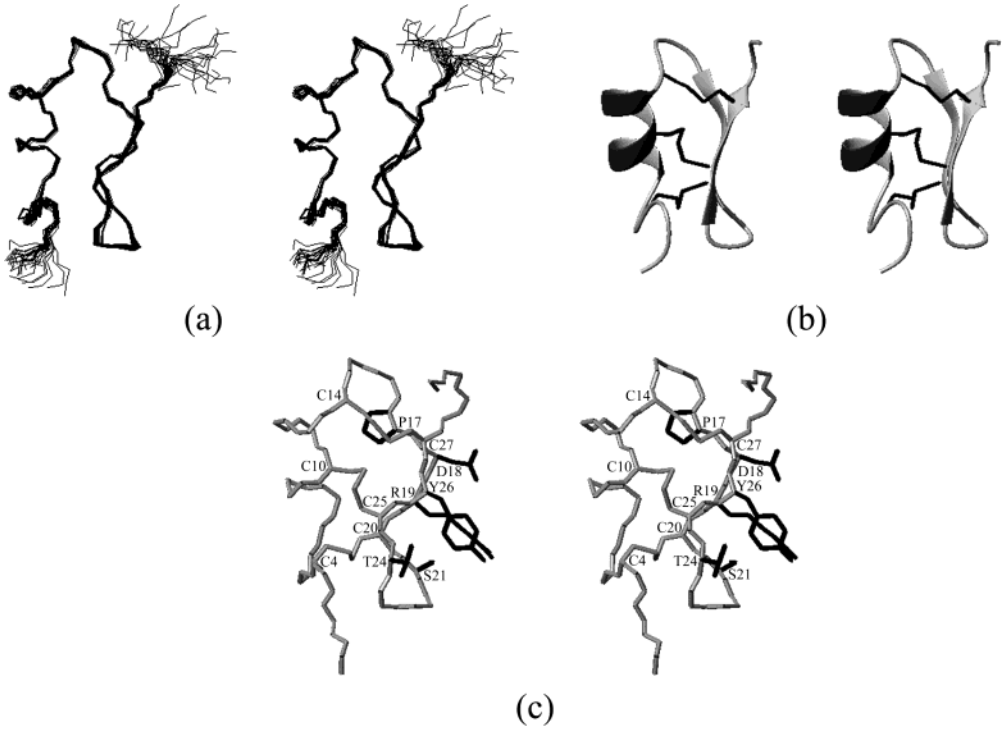


FIGURE 3: (a) Stereoview of the backbone superposition of the best 25 structures of BmKK4. (b) Stereoview of the MOLMOL representation of the mean structure of BmKK4. Secondary structural elements are drawn with three disulfide bridges (neons). (c) Stereoview of the MOLMOL representation of the structure of BmKK4 with the lowest energy. Three disulfide bridges are shown as neons (gray). The residues involved in the two-stranded $\beta$-sheet are labeled, and the heavy atoms of their side chains are shown as neons (black) (neons are a display style of bonds that draws the bond as cylinder with round ends).

Table 1: Structural Statistics for BmKK4

| | | | |
|---|---|---|---|
| DYANA (35 Best Structures) | | | |
| target function (Å$^2$) | $0.0647 \pm 0.00518$ | av no. of angle restraints | 0.0 |
| av no. of upper restraints | 0.0 | violations >5°/structure | |
| violations >0.2 Å/structure | | max violation (deg) | 0.02 |
| max violation (Å) | 0.14 | | |
| AMBER (25 Best Structures) | | | |
| total energy (kcal/mol) | $-335.5 \pm 9.8$ | rmsd from mean coordinates | |
| bond energy (kcal/mol) | $10.1 \pm 0.5$ | all backbone atoms (Å) | $1.09 \pm 0.33$ |
| angle energy (kcal/mol) | $60.0 \pm 2.5$ | all heavy atoms (Å) | $1.87 \pm 0.30$ |
| dihed energy (kcal/mol) | $76.2 \pm 4.7$ | backbone atoms (residues 2−28) (Å) | $0.35 \pm 0.09$ |
| vdwaals energy (kcal/mol) | $-61.2 \pm 3.7$ | heavy atoms (residues 2−28) (Å) | $1.38 \pm 0.21$ |
| eel energy (kcal/mol) | $-431.0 \pm 10.1$ | structure analysis (%) | |
| H bond energy (kcal/mol) | $-11.6 \pm 1.1$ | residues in most favored regions | 77.8 |
| constraint energy (kcal/mol) | $22.0 \pm 1.2$ | residues in allowed regions | 19.7 |
| rmsd from idealized geometry | | residues in generously allowed regions | 2.2 |
| bonds (Å) | $0.0093 \pm 0.00018$ | residues in disallowed regions | 0.3 |
| angles (deg) | $2.29 \pm 0.047$ | | |

Figure 3b shows the mean structure of BmKK4 obtained from the best 25 conformers. The molecule adopts the $\alpha/\beta$-motif, which consists of a double-stranded antiparallel $\beta$-sheet anchored to a single $\alpha$-helix (Val7−Cys14) by two disulfide bridges (Cys10−Cys25 and Cys14−Cys27). The $\alpha$-helix and $\beta$-sheet were linked by a tight turn. The $\beta$-sheet involves residues Pro17−Ser21 (strand I) and Thr24−Cys27 (strand II), which are connected by a type I′ $\beta$-turn (Ser21−Thr24).

It is notable that the regular arrangements of the strands in the $\beta$-sheet of BmKK4 are distorted by a $\beta$-bulge composed of residues Asp18, Arg19, and Tyr26 as shown in Figure 3c. The bulge is identified by the hydrogen bond pattern, in which the amide protons of two consecutive residues (Asp18 and Arg19) hydrogen bond to the oxygen of residue Tyr26 and the amide proton of residue Tyr26 hydrogen bonds to the oxygen atom of Arg19. The $\beta$-bulge is further characterized as a classic type on the basis of the $\phi$ and $\psi$ torsion angle values (data not shown) (*35*).

## DISCUSSION

*Structural Features of BmKK4*. BmKK4 adopts a common $\alpha/\beta$-motif, but shows a distinctive local conformation especially in the $\beta$-sheet and tight turn region between the $\alpha$-helix and $\beta$-sheet as compared with other typical $K^+$ toxins (Figure 4a). The most novel feature is that the regular arrangements of the side chains of the residues involved in the $\beta$-sheet of BmKK4 are distorted by a classic $\beta$-bulge structure, which involves two residues (Asp18 and Arg19) in the first strand opposite a single residue (Tyr26) in the second strand. The bulge produces two main changes in the structure of the antiparallel $\beta$-sheet: (1) It disrupts the normal alteration of the side chain direction; the side chain of Asp18 turns over to form a salt bridge with that of Arg19. (2) It accentuates the twist of the sheet, and alters the direction of

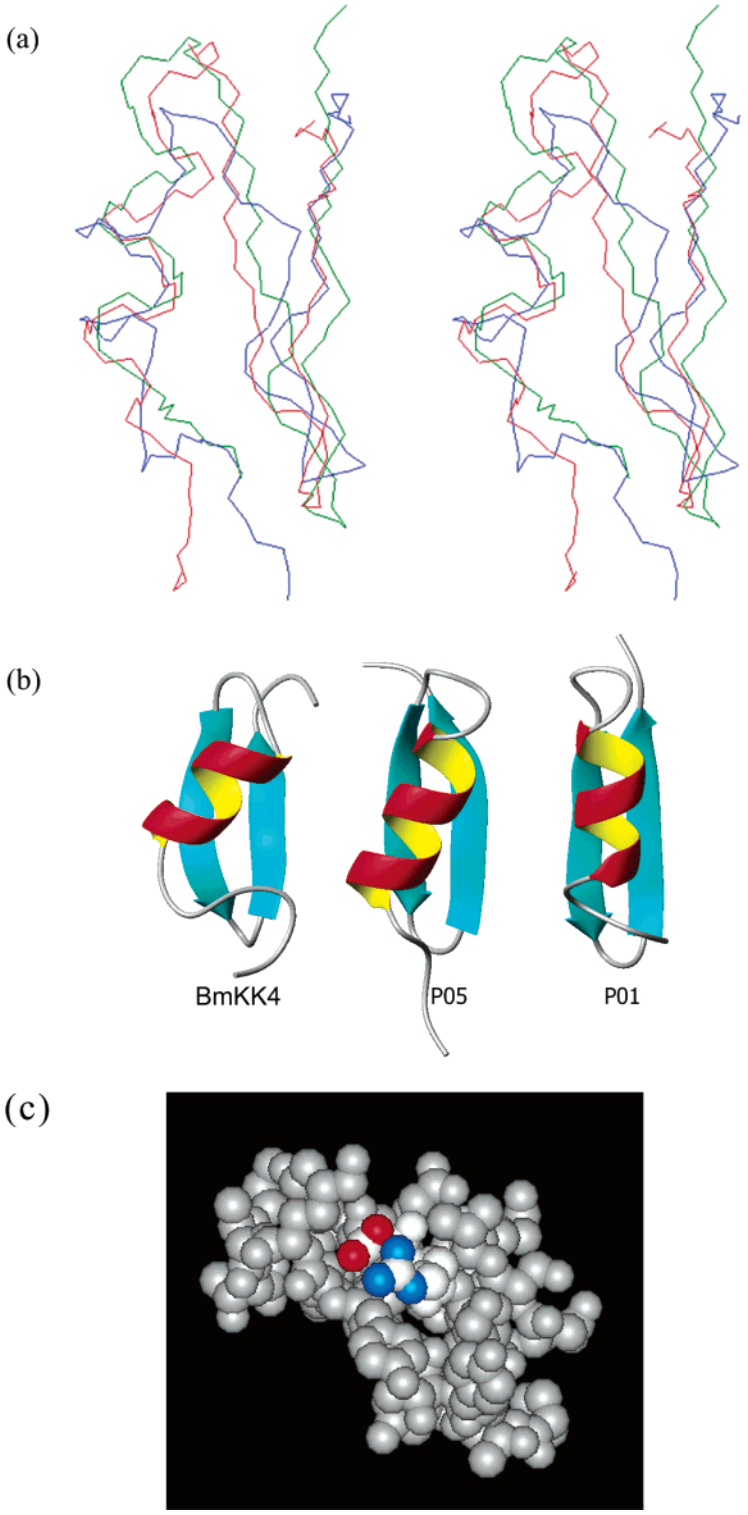


FIGURE 4: (a) Stereoview of the backbone superposition of BmKK4 (in blue), P05 (in red), and P01 (in dark green). P05 and P01 coordinates were obtained from the Protein Data Bank with accession nos. 1PNH and 1ACW, respectively. (b) MOLMOL representation of the structures of BmKK4, P05, and P01. (c) A view of the BmKK4 structure with the salt bridge illustration between the Lys19 residue (with the nitrogen atom in blue) and Asp 18 (with the oxygen atom in red).

the antiparallel $\beta$-sheet. Actually, BmKK4 has a quite large angle ($\sim$45°) between the α-helix and $\beta$-sheet as compared with P05 and P01, in which their helices run nearly parallel to the $\beta$-sheet with a cross-angle of $\sim$10° and $\sim$0°, respectively (Figure 4b).

These structural features in the 3D structure are closely related to the primary sequence of BmKK4. According to the sequence alignment of BmKK4 with other short-chain scorpion toxins as shown in Figure 5, the most distinctive in the sequence of BmKK4 is that two unique residues (Asp18 and Arg19) appeared at the position immediately preceding the fourth Cys residue.

It was suggested by Bontems et al. (*36*) that Cys-[···]-Cys-x-x-x-Cys-[···]-*Gly*-x-Cys-[···]-Cys-x-Cys is the signature sequence for scorpion toxins with the α/$\beta$-motif and the Gly residue at this position is highly conserved due to

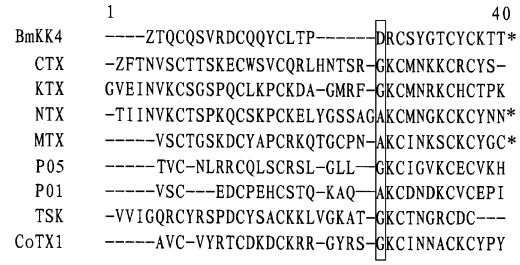


FIGURE 5: Sequences alignment of BmKK4 with those of other similar short-chain scorpion $K^+$ toxins. The amino acid sequences are aligned according to their Cys residues. An asterisk indicates amidation at the C-terminus. Gaps are presented as dashes.

steric hindrance between the helix and sheet. Later studies showed that an Ala residue in this position is also acceptable, as in toxins NTX, MTX, and P01, and the methyl side chain of the Ala residue could be accommodated when the helix is bent slightly (*37*). The replacement of Gly by Asp at position 18 of the toxin BmKK4 should have a big influence on the solution conformation of the molecule. In fact, it leads to the formation of the bulge structure in the $\beta$-sheet moiety, which makes residue Asp18 acceptable by moving its hydrophilic side chain away from the hydrophobic core into the solvent. This kind of arrangement of the side chains of residues Asp18 and Arg19 in the $\beta$-sheet is stabilized by the salt bridge formed between them. In addition, residue Pro17 immediately preceding position 1 of the bulge may be interpreted as another factor in bulge formation. The inability of the Pro residue to take part in the formation of a hydrogen bond residue pair in the antiparallel $\beta$-strand may also cause subsequent residues in the strand to form a bulge. Moreover, the large cross-angle between the α-helix and $\beta$-sheet may also be preferred to avoid the overlap of the α-helix with the bulky side chain of Pro17, which is located at the head of the $\beta$-sheet with its side chain opposite that of Asp18.

On the other hand, in the typical short-chain scorpion toxins the residue preceding the fourth Cys residue usually is a Lys residue, which is crucial for the pore-blocker-type interaction and plugs into the pore and selective filter of the $K^+$ channel. However, in BmKK4 an Arg residue appeared at this position, which is very unusual in short-chain scorpion toxins. In addition, the side chain of Arg19 is not straightly extended, but is in a bend orientation due to its forming a salt bridge with residue Asp18 in the $\beta$-bulge structure (see Figure 4c). Therefore, it is likely that BmKK4 is not a good blocker for the pore-blocking interaction with $K^+$ channels due to the bigger volume of the side chain of residue Arg19 and its bent orientation.

In BmKK4, the amide H/D exchange rate of the residues involved in the $\beta$-sheet is much faster as compared with the usual rates observed for related molecules (*23*, *38*). This instability of the $\beta$-sheet in BmKK4 indicated by H/D exchange experiments could be well explained by the reduction of hydrophobic interactions between the α-helix and $\beta$-sheet. Compared with those of P05 and P01, the bigger cross-angle between the α-helix and $\beta$-sheet in BmKK4 reduced the interaction surface and hydrophobic interactions as well. On the other hand, the conformation of the peptide segment in the N-terminus appears as a loop toward the $\beta$-sheet. Besides, two hydrogen bonds (Gln3 NH···Gly23 O and Cys25 NH···Gln3 OE1) between these two elements are identified. It is clear that the instability of the $\beta$-sheet structure in BmKK4 caused by the reduction of the interaction surface between the α-helix and $\beta$-sheet could be partly compensated by the interactions between its N-terminal residues and the exposed region in the $\beta$-sheet structure.

It is notable that the RMSD values from the idealized geometry for the bonds and angles of the peptide are relatively high as shown in Table 1. This could be mainly attributed to the unique N-terminus of the peptide, which is enveloped by a pyroglutamic residue. A similar situation was found in scorpion toxin BmTX2 (the RMSD values of the bonds and angles are 0.0083 Å and 2.79°), in which the N-terminus is also enveloped by a pyroglutamic residue (*25*). When the first two amino acid residues in the N-terminus of BmKK4 were not taken into account, the RMSD values for the bonds and angles in this case were reduced to 0.0054 Å and 0.794°, respectively.

*Correlation of the Structural Features with the Lower Affinity for the Kv Channel*. In the electrophysiological experiment described by Li et al. (*33*), 10−100 $\mu$M BmKK4 reversibly inhibited both the delayed rectifier and fast transient potassium current in concentration-dependent manners. The affinity for the Kv channel is remarkably lower than that of other members in the α-KTx family. The lower action of this peptide appears to relate to the structural features of the molecule. As discussed above, an Arg residue instead of a lysine at the critical position is unfavorable for binding to the Kv channel. A similar phenomenon has been observed in two natural short-chain peptides (Pi4 and Pi7) isolated from the venom of the scorpion *Pandinus imperator*. Pi4 with a critical residue Lys26 is a potent blocker of the Shaker B $K^+$ channel (Kv1.1 channel), whereas peptide Pi7, in which Arg26 replaces the residue Lys26, is inactive toward the Kv channel (*39*). Similarly, as reported by Goldstein et al., the mutant Lys27Arg of charybdotoxin (ChTx) shows a decrement of 3 orders of magnitude in its affinity for a Shaker-type $K^+$ channel as compared with the wild-type peptide (*16*). Thus, it is clear that the Arg residue at the critical position for binding with the Kv channel is unfavorable. But, the mutant Lys27Arg of ChTx still has a $K_d$ in the nanomolar range contrary to the present case, in which the potency is as low as in the micromolar range. On the other hand, an interesting finding was obtained with a pair of natural scorpion toxins, Pi2 and Pi3, which have a critical residue Lys24 in common and differ only by a single amino acid residue: Pro7 in Pi2 vs Glu7 in Pi3 (*40*). In Pi3 a salt bridge between the crucial residue Lys24 and Glu7 was identified to decrease 20-fold the affinity for the channel as compared to that of Pi2, where position 7 is occupied by a Pro residue. It was interpreted that the intramolecular salt bridge reduced the local positive electrostatic potential around the pore-blocking residue Lys24, resulting in decreased short-range electrostatic interactions during the binding step, and eventually resulting in the lower potency (*41*). This deduction was further supported by the fact that a mutant Ser10Asp of ChTx, where the equivalent residues of Asp10 and Lys27 are Glu7 and Lys24 in Pi3, decreases the affinity for the channel by about 1500-fold (*16*). These facts suggest that the lower activity of BmKK4 toward the Kv channel could be attributed to the combination of the unusual residue Arg19 and the intramolecular salt bridge between itself and Asp18 in the bulge structure of the $\beta$-sheet.

## CONCLUSION

The solution structure of BmKK4, the first member of α-KTx subfamily 17, has been determined by 2D NMR spectroscopy in this study. The most novel structural feature of the molecule is the presence of a classic $\beta$-bulge in the antiparallel $\beta$-sheet. It not only disrupts the normal alternation of the side chain direction of residues involved in the $\beta$-sheet, but also accentuates the twist of the sheet and alters the direction of the $\beta$-sheet secondary structure. Meanwhile, the critical residue Arg19 instead of a Lys residue at the position preceding the fourth Cys is unfavorable for binding with the Kv channel as a pore blocker. Furthermore, the intramolecular salt bridge between Arg19 and Asp18 should be another determinant for the low affinity of the molecule for the Kv channel. The exact target and the mechanism underlying BmKK4-induced inhibition of the $K^+$ current remain to be further investigated.

## ACKNOWLEDGMENT

We thank the Institute of Molecular Biology and Biophysics, ETH-Hönggerberg, Zürich, Switzerland, for providing the programs DYANA (version 1.5) and XEASY. We are grateful to Prof. Bertini of Florence University, Italy, for providing the program CALIBA, Prof. James W. Caldwell of the University of California, San Francisco, for the program AMBER, and Prof. T. A. Jones of Uppsala University, Sweden, for the software program "O". We are also grateful to Tripos, Inc. for the Sybyl6.3 software package.

## REFERENCES

1. Coetzee, W. A., Amarillo, Y., Chiu, J., Chow, A., Lau, D., McCormack, T., Moreno, H., Nadal, M. S., Ozaita, A., Pountney, D., Saganich, M., Vega-Saenz De Miera, E., and Rudy, B. (1999) Molecular diversity of $K^+$ channels, *Ann. N. Y. Acad. Sci. 868*, 233−285.
2. MacKinnon, R., Heginbotham, L., and Abramson, T. (1990) Mapping the receptor site for charybdotoxin, a pore-blocking potassium channel inhibitor, *Neuron 5*, 767−771.
3. MacKinnon, R., Aldrich, R. W., and Lee, A. W. (1993) Functional stoichiometry of Shaker potassium channel inactivation, *Science 262*, 757−759.
4. Olivera, B. M., Hillyard, D. R., Marsh, M., and Yoshikami, D. (1995) Combinatorial peptide libraries in drug design: lessons from venomous cone snails, *Trends Biotechnol. 13*, 422−426.
5. Garcia, M. L., Gao, Y., McManus, O. B., and Kaczorowski, G. J. (2001) Potassium channels: from scorpion venoms to high-resolution structure, *Toxicon 39*, 739−748.
6. Rodriguez de la Vega, R. C., Merino, E., Becerril, B., and Possani, L. D. (2003) Novel interactions between K+ channels and scorpion toxins, *Trends Pharmacol. Sci. 24*, 222−227.
7. Xu, C. Q., Zhu, S. Y., Chi, C. W., and Tytgat, J.(2003) Turret and pore block of K+ channels: what is the difference? *Trends Pharmacol. Sci. 24*, 446−448.
8. Zhu, S., Huys, I., Dyason, K., Verdonck, F., and Tytgat, J. (2004) Evolutionary trace analysis of scorpion toxins specific for K-channels, *Proteins 54*, 361−370.
9. Rodriguez de la Vega R. C., and Possani L. D. (2004) Current views on scorpion toxins specific for $K^+$-channels, *Toxicon 43*, 865−875.
10. Mouhat S., Jouirou B., Mosbah A., De Waard M., and Sabatier J. M. (2004) Diversity of folds in animal toxins acting on ion channels. *Biochem. J. 378*, 717−726.
11. Tytgat, J., Chandy, K. G., Garcia, M. L., Gutman, G. A., Martin-Eauclaire, M. F., van der Walt, J. J., and Possani, L. D. (1999) A unified nomenclature for short-chain peptides isolated from scorpion venoms: alpha-KTx molecular subfamilies, *Trends Pharmacol. Sci. 20*, 444−447.
12. Corona, M., Gurrola, G. B., Merino, E., Cassulini, R. R., Valdez-Cruz, N. A., Garcia, B., Ramirez-Dominguez, M. E., Coronas, F. I., Zamudio, F. Z., Wanke, E., and Possani, L. D. (2002) A large number of novel Ergtoxin-like genes and ERG K+-channels blocking peptides from scorpions of the genus Centruroides, *FEBS Lett. 532*, 121−126.
13. Goudet, C., Chi, C.-W., and Tytgat, J. (2002) An overview of toxins and genes from the venom of the Asian scorpion *Buthus martensi* Karsch, *Toxicon 40*, 1239−1258.
14. Batista, C. V. F., Gomez-Lagunas, F., Rodriguez de la Vega, R. C., Hajduc, P., Panyi, G., Gaspar, R., and Possani, L. D. (2002) Two novel toxins from the Amazonian scorpion *Tityus cambridgei* that block Kv1.3 and *Shaker* B $K^+$-channels with distinctly different affinities, *Biochim. Biophys. Acta 1601*, 123−131.
15. Cai, Z., Xu, C. Q., Xu, Y. Q., Lu, W. Y., Chi, C. W., Shi, Y. Y., and Wu, J. H. (2004) Solution structure of BmBKTx1, a new BKCa1 channel blocker from the Chinese scorpion Buthus martensi Karsch, *Biochemistry 43*, 3764−3771.
16. Goldstein, S. A. N., Pheasant, D. J., and Miller, C. (1994) The charybdotoxin receptor of a Shaker K+ channel: peptide and channel residues mediating molecular recognition, *Neuron 12*, 1377−1388.
17. Gross, A., and MacKinnon, R. (1996) Agitoxin footprinting the Shaker potassium channel pore, *Neuron 16*, 399−406.
18. Naranjo, D., and Miller, C. (1996) A strongly interacting pair of residues on the contact surface of charybdotoxin and a Shaker K+ channel, *Neuron 16*, 123−130.
19. Naini, A. A., and Miller, C. (1996) A Symmetry-Driven Search for Electrostatic Interaction Partners in Charybdotoxin and a Voltage-Gated K+ Channel, *Biochemistry 35*, 6181−6187.
20. Fu, W., Cui, M., Briggs, J. M., Huang, X., Xiong, B., Zhang, Y., Luo, X., Shen, J., Ji, R., Jiang, H., and Chen, K. (2002) Brownian dynamics simulations of the recognition of the scorpion toxin maurotoxin with the voltage-gated potassium ion channels, *Biophys. J. 83*, 2370−2385.
21. Gao, Y.-D., and Garcia, M. L. (2003) Interaction of Agitoxin2, Charybdotoxin, and Iberiotoxin with Potassium Channels: Selectivity between Voltage-Gate and Maxi-K channels, *Proteins 52*, 146−154.
22. Bontems, F., Roumestand, C., Boyot, P., Gilquin, B., Doljansky, Y., Menez, A., and Toma, F. (1991) Three-dimensional structure of natural charybdotoxin in aqueous solution by 1H-NMR. Charybdotoxin possesses a structural motif found in other scorpion toxins, *Eur. J. Biochem. 196*, 19−28.
23. Meunier, S., Bernassau, J. M., Sabatier, J. M., Martin-Eauclaire, M. F., Van Rietschoten, J., Cambillau, C., and Darbon, H. (1993) Solution structure of P05−NH2, a scorpion toxin analog with high affinity for the apamin-sensitive potassium channel, *Biochemistry 32*, 11969−11976.
24. Dauplais, M., Gilquin, B., Possani, L. D., Gurrola-Briones, G., Roumestand, C., and Menez, A. (1995) Determination of the three-dimensional solution structure of noxiustoxin: analysis of structural differences with related short-chain scorpion toxins, *Biochemistry 34*, 16563−16573.
25. Blanc, E., Romi-Lebrun, R., Bornet, O., Nakajima, T., and Darbon, H. (1998) Solution structure of two new toxins from the venom of the Chinese scorpion *Buthus martensi* Karsch blockers of potassium channels, *Biochemistry 37*, 12412−12418.
26. Wu, G., Li, Y., Wei, D., He, F., Jiang, S., Hu, G., and Wu, H. (2000) Solution structure of BmP01 from the venom of scorpion *Buthus martensii* Karsch, *Biochem. Biophys. Res. Commun. 276*, 1148−1154.
27. Wang, I., Wu, S.-H., Chang, H.-K., Shieh, R.-C., Yu, H.-M., and Chen, C. (2002) Solution structure of a K(+)-channel blocker from the scorpion Tityus cambridgei, *Protein Sci. 11*, 390−400.
28. Korolkova, Y. V., Bocharov, E. V., Angelo, K., Maslennikov, I. V., Grinenko, O. V., Lipkin, A. V., Nosyreva, E. D., Pluzhnikov, K. A., Olesen, S. P., Arseniev, A. S., and Grishin, E. V. (2002) New binding site on common molecular scaffold provides HERG channel specificity of scorpion toxin BeKm-1, *J. Biol. Chem. 277*, 43104−43109.
29. Guijarro, J. I., M'Barek, S., Gomez-Lagunas, F., Garnier, D., Rochat, H., Sabatier, J. M., Possani, L. D., and Delepierre, M. (2003) Solution structure of Pi4, a short four-disulfide-bridged scorpion toxin specific of potassium channels, *Protein Sci. 12*, 1844−1854.
30. Jouirou, B., Mosbah, A., Visan, V., Grissmer, S., M'Barek, S., Fajloun, Z., Van Rietschoten, J., Devaux, C., Rochat, H., Lippens, G., El Ayeb, M., De Waard, M., Mabrouk, K., and Sabatier, J.

M. (2004) Cobatoxin 1 from Centruroides noxius scorpion venom: chemical synthesis, three-dimensional structure in solution, pharmacology and docking on K+ channels, *Biochem. J. 377*, 37−49.
31. Zhang, N. X., Li, M. H., Chen, X., Wang, Y. F., Wu, G., Hu, G. Y., and Wu, H. M. (2004) Solution structure of BmKK2, a new potassium channel blocker from the venom of chinese scorpion Buthus martensi Karsch, *Proteins 55*, 835−845.
32. Zhang, N. X., Wu, G., Wu, H. M.,Chalmers, M. J., and Gaskell, S. J. (2004) Purification, characterization and sequence determination of BmKK4, a novel potassium channel blocker from Chinese scorpion *Buthus martensi* Karsch, *Peptides 25*, 951−957.
33. Li, M. H., Zhang, N. X., Chen, X. Q., Wu, G., Wu, H. M., and Hu, G. Y. (2003) BmKK4, a novel toxin from the venom of Asian scorpion *Buthus martensi* Karsch, inhibits potassium currents in rat hippocampal neurons in vitro, *Toxicon 42*, 199−205.
34. Wüthrich, K. (1986) *NMR of Proteins and Nucleic Acid*, John Wiley & Sons, New York.
35. Chan, A. W., Hutchinson, E. G., Harris, D., and Thornton, J. M. (1993) Identification, classification, and analysis of beta-bulges in proteins, *Protein Sci. 2*, 1574−1590.
36. Bontems, F., Roumestand, C., Gilquin, B., and Toma, F. (1991) Refined structure of charybdotoxin: common motifs in scorpion toxins and insect defensins, *Science 254*, 1521−1523.
37. Blanc, E., Sabatier, J. M., Kharrat, R., Meunier, S., el Ayeb, M., Van Rietschoten, J., and Darbon, H. (1997) Solution structure of maurotoxin, a scorpion toxin from Scorpio maurus, with high affinity for voltage-gated potassium channels, *Proteins 29*, 321−333.
38. Blanc, E., Fremont, V., Sizun, P., Meunier, S., Van Rietschoten, J., Thevand, A., Bernassau, J.-M., and Darbon, H. (1996) Solution structure of P01, a natural scorpion peptide structurally analogous to scorpion toxins specific for apamin-sensitive potassium channel, *Proteins 24*, 359−369.
39. Olamendi-Portugal, T., Gomez-Lagunas, F., Gurrola, G. B., and Possani, L. D. (1998) Two similar peptides from the venom of the scorpion Pandinus imperator, one highly effective blocker and the other inactive on K channels, *Toxicon 36*, 759−770.
40. Gomez-Lagunas, F., Olamendi-Portugal, T., Zamudio, F. Z., and Possani, L. D. (1996) Two novel toxins from the venom of the scorpion Pandinus imperator show that the N-terminal amino acid sequence is important for their affinities towards Shaker B K+ channels, *J. Membr. Biol. 152*, 49−56.
41. Peter, M., Jr., Varga Z., Hajdu, P., Gaspar, R., Jr., Damjanovich, S., Horjales, E., Possani, L. D., and Panyi, G. (2001) Effects of toxins Pi2 and Pi3 on human T lymphocyte Kv1.3 channels: the role of Glu7 and Lys24, *J. Membr. Biol. 179*, 13−25.

BI0490643